Precision Measurement of the Lifetime of the $3d\,^2D_{5/2}$ state in $^{40}Ca^+$

P. A. Barton, C. J. S. Donald, D. M. Lucas, D. A. Stevens, A. M. Steane, D. N. Stacey
Centre for Quantum Computation, Department of Atomic and Laser Physics, University of Oxford,
Clarendon Laboratory, Parks Road, Oxford OX1 3PU, England.

10 February, 2000

Abstract

We report a measurement of the lifetime of the $3d\,^2D_{5/2}$ metastable level in $^{40}Ca^+$, using quantum jumps of a single cold calcium ion in a linear Paul trap. The $4s\,^2S_{1/2}$–$3d\,^2D_{5/2}$ transition is significant for single-ion optical frequency standards, astrophysical references, and tests of atomic structure calculations. We obtain $\tau = 1.168 \pm 0.007$ s from observation of nearly 64,000 quantum jumps during ~ 32 hours. Our result is more precise and significantly larger than previous measurements. Experiments carried out to quantity systematic effects included a study of a previously unremarked source of systematic error, namely excitation by the broad background of radiation emitted by a semiconductor diode laser. Combining our result with atomic structure calculations yields 1.20 ± 0.01 s for the lifetime of $3d\,^2D_{3/2}$. We also use quantum jump observations to demonstrate photon anti-bunching, and to estimate background pressure and heating rates in the ion trap.

1 Introduction

In this paper we present a measurement of the natural lifetime τ of the $3d\,^2D_{5/2}$ metastable level in singly-ionised calcium, using quantum jumps of a single cold calcium ion in a linear Paul trap. The $3D_{5/2}$ level is of interest as the source of an optical frequency standard at 729 nm with $1/\tau \sim 1$ Hz natural linewidth [1], as a means of testing atomic structure calculations [2, 3, 4, 5, 6, 7, 8], and as a diagnostic in astrophysics [9, 3]. In addition, our experiments offer insights into the diagnostics on the performance of the Paul trap, and highlight the need to take into account the spectral properties of semiconductor diode laser emission when such devices are used in atomic physics experiments.

Our result is $\tau = 1.168 \pm 0.007$ s, and is shown together with other recent measurements and theoretical predictions in figure 1. Our result is higher (a longer lifetime) than all the previous measurements, and differs by several standard deviations from most of them. It is possible that this discrepancy is at least partly due to a previously unrecognised source of systematic error, namely the presence of light of wavelength in the vicinity of 854 nm in the beam produced by a semiconductor diode laser emitting predominantly at 866 nm. This is discussed in section 4.1.

Precise knowledge of atomic structure for atoms or ions with a single electron outside closed shells is currently in demand for the analysis of atomic physics tests of electroweak theory, especially measurements of parity violation in Cs [10]. There has been a long-standing discrepancy at the 2% level between measured and theoretically predicted rates for electric dipole transitions [11]. Up until now measurements of the metastable lifetimes (electric quadrupole transition rates) in Ca^+ have not been sufficiently precise to provide an independent test of *ab initio* calculations at this level of precision. Our measurement precision is 0.6 %. Furthermore the electric quadrupole transition rate is harder to calculate accurately (recent calculated values have a 15% spread), so our result is of particular interest to atomic structure theory.

The paper is organized as follows. First we discuss, in section 2, the central features of our experimental method to measure τ. Details of the apparatus are provided in section 3. This is a completely new apparatus which has not been described elsewhere, so we give a reasonably full description.

Section 4 presents our study of systematic effects in the experiment. These include collisions with the background gas, off-resonant excitation of the 854 nm $3D_{5/2}$–$4P_{3/2}$ transition and of the 850 nm $3D_{3/2}$–$4P_{1/2}$ transition, heating of the trapped ion, and noise in the fluorescence signal. Section 5 contains a clean demonstration of photon anti-bunching, using the random telegraph method, and section 6 presents the final accurate measurements of τ.

2 Experimental method

The experimental method was identical, in principle, to that adopted by Block *et al.* [12]; preliminary experiments were carried out somewhat differently (see section 5). A single ion of $^{40}Ca^+$ is trapped and laser-cooled to around 1 mK. The transitions of interest are shown in figure 2. Laser beams at 397 nm and 866 nm continuously illuminate the ion, and the fluorescence at 397 nm is detected by a photomultiplier. The photon count signal

is accumulated for periods of duration $t_b = 10.01$ ms (of which 2.002 ms is dead time), and logged. In our studies of systematic effects, and for our demonstration of photon antibunching, t_b was set at 22.022 ms. A laser at 850 nm drives the $3D_{3/2}$–$4P_{3/2}$ transition. The most probable decay route from $4P_{3/2}$ is to the $4S_{1/2}$ ground state; alternatively, the ion can return to $3D_{3/2}$. However, about 1 decay in 18 occurs to $3D_{5/2}$, the metastable "shelving" level of interest. At this point the fluorescence abruptly disappears and the observed photon count signal falls to a background level. A shutter on the 850 nm laser beam remains open for 100 ms before it is closed, which gives ample time for shelving. Between 5 and 10 ms after the shutter has closed, we begin one "observation", i.e., we start to record the photomultiplier count signal (see figure 3a). We keep observing the photon count, in the 10 ms bins, until it abruptly increases to a level above a threshold. This is set between the background level and the level observed when the ion fluoresces continuously. The signature for the end of a dark period is taken to be ten consecutive bins above threshold. We record the number of 10 ms bins in the observed 'dark' period. The 100 ms period of fluoresence also serves to allow the 397 nm and 866 nm lasers to cool the ion. After this we re-open the shutter on the 850 nm laser. This process is repeated for long periods of time (1 to 8 hours), the laser intensities being also monitored and the frequencies servo-controlled. Subsequent analysis of the large collection of dark times consists primarily of gathering them into a histogram, and fitting the expected exponential distribution, in order to derive the decay rate from the shelved state (see figure 4).

Note that we do not measure the length of the dark period from when the ion is first shelved. This is not necessary, since the probability of decay is independent of how long the ion has been in the metastable state. This gives us time to block the 850 nm light, in order to prevent both off-resonant excitation of the ion by this light, and the possibility of missed quantum jumps should this light rapidly (in less than 5 ms) re-shelve a decayed ion.

The data from a given run were analysed as follows. The raw data consist of a series of counts indicating the average fluorescence level in each bin of duration t_b. A threshold is set, typically at $(2S_{\rm dark} + S_{\rm bright})/3$, where $S_{\rm dark}$ is the mean count observed during dark periods, and $S_{\rm bright}$ the mean count observed during fluorescing periods. This setting is chosen because bright periods have more noise than dark periods. The number of consecutive bins below threshold is a single dark-time measurement x_i. The x_i are expected to be distributed according to the exponential decay law, with Poissonian statistics describing the departures from the mean. It is appropriate to use a Poissonian fitting method, rather than least squares, because of the small numbers involved in part of the distribution (at large t). If $n(t_i)$ is the number of x_i equal to t_i/t_b then the cost function is

$$-\ln\left[\prod_{i=0}^{m} P\left(n(t_i)\right)\right] = \sum_{i=0}^{m}\left[Ae^{-\gamma t_i} + \ln\left(n(t_i)!\right) - n(t_i)\ln A + n(t_i)\gamma t_i\right] \quad (1)$$

where m is the number of bins, and A and γ are two fitted parameters (obtained by minimising the cost function); they are the amplitude and decay rate in the assumed exponential decay $A\exp(-\gamma t)$ of population of $D_{5/2}$. The residuals shown in figure 4 indicate that our data are well fitted by an exponential function. Only dark times of duration less than 5 s are included in the fit, since our data collection procedure misses some dark times longer than this. We found that the statistical error in the fitted parameters was consistent with the expected $\sqrt{N}/N$ value, where N is the number of x_i in the whole data set.

3 Apparatus

We use a linear radio-frequency (r.f.) Paul trap, combined with an all-diode laser system, to isolate and cool a single ion of $^{40}Ca^{+}$. The electrodes are made from stainless steel rods and mounted on two supports made from machinable ceramic (Macor); an end view is shown in figure 5. The radial r.f. electrodes, of diameter 1.2 mm, are centred at the corners of a square of side 2.6 mm. The d.c. endcap electrodes, of diameter 1.0 mm are centred on the z-axis and positioned 7.2 mm apart. In addition to the electrodes which comprise the trap, there are a further four 1.6 mm diameter electrodes positioned in a similar configuration to that of the r.f. electrodes, but centred at the corners of a 8.4 mm square. These electrodes allow potentials to be added to compensate for stray electric fields in the trapping region.

The complete experimental apparatus is shown schematically in figure 6, to which we refer in the remainder of this section. The trap electrodes lie at the centre of a hexagonal stainless steel vacuum chamber. A high-voltage a.c. source RF supplies a drive voltage of frequency 6.2 MHz and peak-to-peak amplitude 135 V for the radial electrodes, while high-voltage d.c. supplies DC provide the voltages for the endcaps (95 V in the present experiments) and compensation electrodes (typically around 60 V are applied to the upper two compensation electrodes, while the lower two are grounded).

The central chamber is pumped by a 25 l/s ion pump IP and a 30 l/s getter pump GP. An ion gauge IG on the opposite side of the main chamber monitors the pressure; this is below 2×10^{-11} torr, the limit of the gauge's sensitivity. To produce calcium ions in the trapping region, we use a calcium oven c and electron gun e. The oven is a thin-walled stainless steel tube filled with calcium granules, closed by crimping at each end and with a small hole at the centre pointing towards the trap region. The oven is heated by passing a 6 A current along its length, which produces a

beam of calcium atoms. The electron gun consists of a tungsten filament, also resistively heated, enclosed within a grounded stainless steel "grid" with respect to which it is negatively biased by 50 V. To load the trap, the oven and electron gun are heated for a few minutes, the latter being left on for 10 s after the oven has been turned off. We capture a small cloud of approximately 10 calcium ions using this procedure. This cloud is reduced to a single ion by applying to one of the endcaps a low-voltage "tickle" oscillation, close to the axial resonance frequency of the trap, expelling ions until only one remains in the trap.

Violet light at 397 nm is generated by frequency-doubling 794 nm light from a master-slave diode laser system. A grating-stabilized master diode 794M, with a linewidth below 1 MHz, is locked to a stabilized low-finesse reference cavity RC and used to inject a slave diode 794S. Light from the slave is frequency-doubled by a 10 mm long Brewster-cut lithium triborate crystal LBO in an external enhancement cavity; Hänsch-Couillaud polarization analysis of light reflected by the cavity provides a feedback signal for a piezo-mounted mirror PZT used to lock the cavity length to the fundamental light. The measured characteristics of the doubling cavity are: finesse 130, enhancement 43, mode-matching efficiency 94%, input power 90 mW at 794 nm, output power 0.50 mW at 397 nm. Correcting for losses at the exit face of the crystal and the output coupler gives an internal crystal efficiency $\gamma = 54(5)\,\mu\mathrm{W/W}^2$, some 20% greater than previously reported values [13, 14] and about 75% of the theoretical optimum efficiency calculated using a Boyd-Kleinman analysis [15] and an effective non-linear coefficient for LBO of $d_{\mathrm{eff}} = 0.855\,\mathrm{pm/V}$ [16]. The 397 nm beam passes through a $\lambda/2$ waveplate and polarizing beam splitter (PBS) cube to provide intensity control, and a lens focuses it to a spot size of $200 \times 30\,\mu$m (measured with a CCD camera) at the centre of the trap. The beam power used is typically 0.2 mW.

A grating-stabilized diode laser 866 provides repumping light at 866 nm whose intensity is adjusted by a $\lambda/2$ waveplate and PBS cube. A heated iodine bromide vapour cell IBr provides an absolute frequency reference—unfortunately not suitable for reliable locking—and a triple-pass acousto-optic modulator AOM shifts the laser light some 650 MHz into resonance with the $3D_{3/2} \rightarrow 4P_{1/2}$ calcium transition. Spontaneous light near 854 nm emitted by the laser diode (see section 4.1.2) is rejected by a diffraction grating DG and aperture A. The transmitted 866 nm light is superimposed on the 397 nm beam using a PBS cube and focused onto the trap. The spot size used in the final lifetime measurements was $250 \times 130\,\mu$m; the maximum beam power was 2 mW.

The light at 850 nm to shelve the ion is provided by a third grating-stabilized laser diode 850 situated on a separate optical table, and is directed into the ion trap via a polarization-preserving monomode optical fibre. The intensity is controlled by a $\lambda/2$ waveplate before the optical isolator. A mechanical shutter S before the fibre allows complete extinction of this light. The spot size at the trap is $450 \times 450\,\mu$m and the maximum power 0.5 mW.

For clarity in figure 6 the detection optics are shown in the plane of the diagram: they are actually vertically above the ion trap. A wide-aperture compound lens gathers fluorescence emitted by the trapped ion and images it onto an aperture to reject scattered light; further lenses re-image the light, via a violet filter, onto a photomultiplier PMT connected to a gated photon counter. The net collection efficiency of the detection system, including the 16% quantum efficiency of the PMT at 397 nm, is approximately 0.12%. The peak photon count rate above background for a single cooled ion is typically 32 kHz.

A personal computer PC is used for data acquisition and control of the experiment; in particular it provides timing, logs PMT count data, controls the shutter S, and eliminates long-term drift of the 866 nm laser by locking it to the fluorescence signal from the trapped ion at the end of each 20 s acquisition period.

4 Searches for systematic effects

We now consider effects which alter the measured shelving periods from those appropriate to an unperturbed ion subject only to spontaneous decay. These are of two distinct types: those which alter the shelving periods themselves, because the ion is perturbed in some way, and those which cause systematic error in the process of measurement. We consider the two in turn. The significant difference between our final result and previous work calls for a detailed discussion here.

4.1 Perturbations to the ion

When the ion is fluorescing, it is cycling between the levels $4\,^2S_{1/2}$, $4\,^2P_{1/2}$ and $3\,^2D_{3/2}$. We denote this system of levels by Λ. During the shelving period, the ion is subject to radiation from two of the lasers (397 nm and 866 nm), to thermal radiation, and to the fields associated with the trap. There may also be collisions with the background gas. Any of these perturbations can transfer the ion to the Λ system. We consider them in turn.

4.1.1 Electric field

The ion experiences a static electric field because of imperfect compensation. The most significant effect on the internal state of the ion is to mix the $3D_{5/2}$ and $4P_{3/2}$ levels, so that the measured lifetime is shortened by the presence of the induced $4P_{3/2}$–$4S_{1/2}$ strong electric dipole transition. In fact, using the known matrix elements, one finds that the effect is negligible; the induced transition probability is $9.0 \times 10^{-14} E^2\ \mathrm{s}^{-1}$, so that a field of 300 kV m^{-1} (three orders of magnitude larger than the typical compensating fields used) would be necessary to produce a 1% reduction in the lifetime. We note, however, that

there is another effect associated with an imperfectly compensated field, that of heating during the shelving period; we consider this in section 4.2.1.

4.1.2 Laser radiation

From the standard theory of atom-light interaction, one finds that transitions from a lower level (1) to a higher level (2) in the multi-level ion can be stimulated by radiation of intensity I and angular frequency ω_L at a rate R_{12} (averaged over all Zeeman components) given by

$$R_{12} = \frac{2J_2+1}{2J_1+1}\frac{\pi^2c^3}{\hbar\omega_{12}^3}A_{21}\frac{I}{c}g(\omega_L-\omega_{12}) \qquad (2)$$

where J_1 and J_2 are the total angular momenta of the levels, ω_{12} is the atomic resonance angular frequency, and $g(\omega_L-\omega_{12})$ is the normalised lineshape function. In our case we may assume Lorentzian lineshapes, so that

$$g(\omega_L-\omega_{12}) = \frac{\Gamma/(2\pi)}{(\omega_L-\omega_{12})^2+\Gamma^2/4} \qquad (3)$$

with the linewidth $\Gamma = 1/\tau_2$ determined by the sum of all the decay processes from the upper level.

Since Block *et al.* [12] reported a significant dependence of the shelving time on the intensity of the repumping laser, we first consider excitation from $3D_{5/2}$ to $4P_{3/2}$ by light at 866 nm. The lifetime τ_2 of the $4P_{3/2}$ level has been measured to be 6.924 ± 0.019 ns [11]. We use the value $A_{21} = (7.7 \pm 0.3) \times 10^6$ s^{-1} from *ab initio* [7] and semiempirical [17] atomic structure calculations. The 4% uncertainty is our own estimate, based on the variation among the published calculations, and on the fact that the calculations produce other electric dipole matrix elements in agreement with experiment to better than this level of precision. In any case a 10% error in the value of A_{21} would have a negligible influence on our final result.

To excite the $3D_{5/2}$–$4P_{3/2}$ transition on resonance would require radiation of wavelength 854 nm. From equation (2), we find that with 866 nm light the rate is 9.9×10^{-5} s^{-1}/mW mm^{-2}. The probability that the ion will subsequently decay back to $3D_{5/2}$ is the branching ratio $b = A_{21}\tau_2 = 0.053$, so the rate at which it will be transferred to the Λ system is $(1-b)R_{12} = 9.4\times10^{-5}$ s^{-1}/mW mm^{-2}. In our experiments, it is convenient to choose the 866 nm intensity such that the $3D_{3/2} \rightarrow 4P_{1/2}$ transition is saturated. This requires $I_{866} \gg 0.08$ mW mm^{-2} if the laser frequency is set on resonance (taking this A_{21} coefficient 8.4×10^6 s^{-1} [7, 17]), but to avoid the need to control this frequency precisely a much higher intensity was used, typically 1.5 mW in a spot size of 250×130 μm, or 30 mW mm^{-2}. This results in a contribution to the depopulation rate of the $3D_{5/2}$ level of around 0.3% of that due to spontaneous emission to the ground level.

This is far smaller than the experimental result of Block *et al.* However, in our own preliminary work we also found that there was a significant dependence of the shelving time on the intensity of the repumper laser, of the same order of magnitude as that reported by Block *et al.*, and some 200 times larger than the theoretical value given above. This suggested that the 866 nm laser was emitting some radiation much closer in wavelength to 854 nm which was primarily responsible for the shortening of the apparent lifetime of the $3D_{5/2}$ level. This laser is a semiconductor diode device, operated with an extended cavity by use of a Littrow-mounted diffraction grating. Without the grating, the laser would operate close to 854 nm. Since any laser produces spontaneous emission over its gain profile, as well as stimulated emission at the lasing wavelength, there was in our preliminary work radiation incident on the ion in the vicinity of 854 nm. One might expect the intensity of this radiation to be greatly reduced because of the long (3m) beam path. In fact, this is not the case, because the emitting region in the laser is small (dimensions of order microns) so the spontaneous component is well collimated; like the coherent component, it is transported to the trap with little loss.

We therefore investigated the spectrum of the light from the laser by means of a diffraction grating, and found it to contain a broad background from 840 nm to 870 nm. When the total laser power near the ion trap was 2 mW, the power in the broad component was 8 μW, and the spot sizes were similar. This implies a mean spectral density around 854 nm sufficient to cause de-shelving rates considerably higher than those we observed; we ascribe the lower observed rates to the structure of the background. This was not resolved in our investigation, but is expected on the basis of other experimental work [18, 19] to include a long series of spikes separated by the longitudinal mode spacing of the diode (50 GHz). These occur because the gain is so high in these devices that there is some amplification right across the gain profile; evidence that this occurs in our laser is provided by the high degree of polarization (90%) of the background. It is thus reasonable to conclude that the $3D_{5/2}$–$4P_{3/2}$ atomic resonance falls between peaks in the 50 GHz spaced comb.

To study the effects of this background radiation we reduced its intensity at the position of the ion. This was done in two stages: first, we reduced it by a factor of 25 using an interference filter centred on 866 nm. The observed de-shelving rate fell from 1.85 ± 0.06 s^{-1} to 0.87 ± 0.02 s^{-1}, the two measurements being taken at the same 866 nm intensity. This provided convincing evidence that the de-shelving was indeed caused by the postulated mechanism. We therefore replaced the filter with a diffraction grating and iris aperture, arranged to pass light at 866 nm. The power transmitted by the system in the vicinity of 854 nm was then reduced compared with the unfiltered laser by three and a half orders of magnitude (for a given intensity at 866 nm), and the remaining light was scattered, thus increasing the illuminated area in the vicinity of the ion by a factor measured to be 40, making a net intensity reduction 8×10^{-6}. Under these conditions transitions stimulated by this radiation become much less probable

than those due to the 866 nm light itself. The observed de-shelving rate was 0.858 ± 0.007 s^{-1}. De-shelving rates γ at various settings of the intensity I of the 866 nm laser beam as measured in these various experiments are shown in figure 7a. A straight line of the form $\gamma = \gamma_0 + \alpha I$ fitted to the points for which the grating and iris system were in place gives $\gamma_0 = 0.857 \pm 0.016$ s^{-1}, $\alpha = (1.5 \pm 6) \times 10^{-3}$ s^{-1}/mW mm^{-2}. The value of γ_0 is consistent with our final more accurate measurements, given in section 6 below, while the slope is consistent with zero (and with the very small theoretical value for de-shelving by 866 nm radiation given above). The intercept with unfiltered light is greater than that given by our final data because our method of varying the laser intensity did not alter the unpolarized component of the background radiation.

Spontaneous emission from the repumper laser appears also to be likely to account for the observations of Block *et al.* It is possible that it was present in previous work on the $3D_{5/2}$ lifetime, and unaccounted for, explaining the lower values obtained by all earlier workers. This does not immediately apply to Block *et al.*, however, because their measurement involved an extrapolation to zero laser intensity using neutral density filters.

The 866 nm laser might also generate radiation near 854 nm if it went multimode owing to a degradation of the alignment of its own external cavity. If intermittent and at a low level, this effect could occur undetected. However, multimode operation was found in practice to have an all-or-nothing character: if it occurred at all then it was obvious from a large increase in the noise of the fluorescence signals, and in such a case the data were discarded.

The grating and iris system were in place for our final data sets. Figure 7b shows our final rate measurements plotted against the intensity of the repumper laser. The observations are consistent with the theoretical value for the slight dependence on 866 nm intensity. Our final result for the lifetime was obtained with a slope fixed at the theoretical value (see section 6).

The radiation at 397 nm is obtained by frequency-doubling and so does not contain any significant background light. There is no transition from $3D_{5/2}$ near enough to this wavelength to cause significant de-shelving. A check for this or some other (unidentified) effect was nevertheless carried out, where we changed the power of this light by a factor 2, and we observed, to ten percent precision, no effect on the deshelving rate.

4.1.3 Thermal radiation

The rate of de-shelving is $(1-b)B_{12}\rho(\omega_{21})$, where $\rho(\omega)$ is the energy density per unit frequency interval in the thermal radiation, and $B_{12} = g_2\pi^2c^3A_{21}/(g_1\hbar\omega_{21}^3)$. In a thermal cavity we obtain the rate

$$(1-b)\frac{2J_2+1}{2J_1+1}A_{21}e^{-\hbar\omega_{21}/k_{\rm B}T} \qquad (4)$$

for $\hbar\omega_{21} \gg k_{\rm B}T$. For the 854 nm transition in a room-temperature cavity, the rate is of order 10^{-18} s^{-1} so is negligible. Non-negligible rates can be obtained, however, when we consider the radiation produced by room lights or the filament of an ion gauge. The spectral energy density is reduced from the value in equation (4) by a geometrical factor approximately equal to $S/(4\pi r^2)$ where S is the area of the hot filament and r is its distance from the ion, if the ion is within line of sight of the filament. For example, taking $T = 1700$ K, $S = 20$ mm^2, $r = 30$ cm, we obtain a rate $\sim 5 \times 10^{-3}$ s^{-1}. In our vacuum system, although the ion gauge is at this distance from the trapped ion, it is not in line of sight, so we expect the rate of this process to be well below this value.

4.1.4 Collisional effects

The ion in the shelved level can undergo a collision with an atom of the background gas. Either or both of two processes may then occur: the ion may gain a significant amount of kinetic energy, and it may be transferred to another state. This is a source of error since in both cases the apparent shelving time — the interval during which fluorescence is not observed — will be affected. To investigate the nature and frequency of collisional effects we monitored the fluorescence from the ion for 8 hours with the 397 nm and 866 nm radiation present but with no laser operating at 850 nm to take the ion to the $4P_{3/2}$ level. The diffraction grating and aperture were in place. During this period we observed abrupt disappearance of the fluorescence (within the resolution of the 22 ms bins) on 17 occasions. It reappeared after times of the order of a second, with 6 "dark periods" as short as a few tens of milliseconds. The reappearance was generally abrupt, but in 5 of the longer periods it was more gradual, occurring over several bins.

One non-collisional effect which can lead to loss of fluorescence in this test is shelving in the $3D_{5/2}$ level. Shelving caused by the 866 nm radiation exciting the $3D_{3/2}$ to $4P_{3/2}$ transition is negligible, because the spontaneous decay to $3D_{5/2}$ has such a low branching ratio (the excitation rate can be calculated from the branching ratio b and the $3D_{3/2} \rightarrow 4P_{3/2}$ coefficient $A_{21} = 0.91 \times 10^6$ s^{-1} [7, 17]). In contrast, it is not possible to rule out excitation by the spontaneously emitted light from the 866 nm laser at 850 nm because the rate depends on the spectral distribution of the spontaneous emission at 850 nm; if a peak happened to be close to the frequency of the 850 nm transition the process could be responsible for a significant number of the observed events. However, we would then expect an abrupt reappearance of the fluorescence on a time scale of the order of a second, and the data then suggest that the upper limit for events of this type is around eight. These could alternatively be caused by fine-structure changing collisions; the ion in the $3D_{3/2}$ level can be transferred to $3D_{5/2}$ by a long range collision which may not transfer significant kinetic energy. At our working pressure of order

10^{-11} mbar we would expect about 8 such events on the basis of an approximate value of the collisional mixing rate which has been determined for conditions similar to ours [20, 21]. Our observations thus provide a rough upper limit on the background gas pressure in our system directly at the location of the ion, to confirm our ion gauge reading. We note that the rates for $D_{5/2} \rightarrow D_{3/2}$ and $D_{3/2} \rightarrow D_{5/2}$ are approximately equal at room temperature, therefore the present experiment does give an indication of the deshelving rate due to fine-structure changing collisions in our $D_{5/2}$ lifetime measurements.

The other events are more obviously characteristic of collisions. In particular, the more gradual reappearance of the fluorescence after a long dark period is likely to be associated with the ion being cooled again after acquiring a significant amount of kinetic energy. On the basis of our measured pressure and reasonable estimates of cross-sections, we do not expect more than two or three collisions of this type. Some of the very short dark periods are likely to be much smaller perturbations by relatively distant collisions. If such a perturbation were to occur during the lifetime measurement itself, fluorescence would not be observable for a period whatever state the ion was in after the collision. Fortunately, for the purposes of estimating the uncertainty in the lifetime measurement, detailed interpretation of the events is not necessary. An upper limit to the error introduced can be found by assuming that all 17 events are due to collisions, giving a rate of 6×10^{-4} s^{-1}, and that such a collision occurring in the experimental runs themselves while the ion was in the shelved level would have delayed (or hastened) the reappearance of fluorescence by an average of order 1 second. The net contribution to the measured rate has thus an upper limit of $\pm 6 \times 10^{-4}$ s^{-1} which is an order of magnitude below the statistical error.

4.2 Systematic effects in the measurement process

Both the fluorescence and the background signal on which it is superposed are subject to fluctuations. As well as the random error this introduces into the measurement, because the instant at which fluorescence resumes is subject to statistical uncertainty, there are systematic effects. For example, a large fluctuation in the background can suggest that the ion has decayed while it is still shelved; our data analysis procedure had to be developed and tested to minimise errors due to such effects. Further, the ion is not cooled during the shelved period, and if there is significant heating the fluorescence may be reduced for a time after the decay.

4.2.1 Heating during the shelved periods

In our preliminary experiments, we found that when an electric field was applied in the vertical direction the fluorescence reappeared only gradually after shelving, over periods of 10–50 ms. We ascribe this to heating. When the d.c. electric field in the trap is not zero, the ion experiences the r.f. driving field, which is much more noisy than the d.c. field, and so the ion motion heats during the shelved periods when it is not laser cooled. We calculate that if the ion heats up to room temperature, it would take the lasers approximately 50 ms to cool the motion down again and thus for the fluorescence to reappear. Evidence supporting this interpretation is given by the fact that the non-abrupt reappearance of fluorescence was correlated to the duration of the dark period, being more likely for longer dark periods. We therefore took care to ensure this phenomenon was not present in the runs used for our final data set. This was done by nulling the vertical field carefully before each run.

In our linear trap geometry the r.f. field is 2-dimensional. To null the vertical field we adjusted the voltage on one of the d.c. field compensation electrodes, so as to minimise the linewidth of the ion fluorescence as a function of 397 nm laser frequency (at lowered 397 nm laser power). The 397 nm laser beam used for shelving measurements enters along the direction $(\sqrt{3}, 0, 1)$ (where the xz plane is horizontal); this is sensitive to horizontal micromotion and hence the vertical field. We were able to null this field to ± 3 V/m, and most runs were carried out with nulling to ± 10 V/m. We measured the remaining heating rate, when this field was as well compensated as we could make it, by blocking the cooling laser beams (397 nm and 866 nm) for long periods, and looking for a non-abrupt return of the fluorescence when the beams were unblocked. No delay was observed (the limit of sensitivity being the bin size of 22 ms) unless the cooling lasers were blocked for more than 10 minutes, some 600 times longer than the shelving times occurring during the measurements themselves. The consequent systematic error in the lifetime can thus be safely neglected; heating is likely to be relatively slow when the ion is first shelved, but even assuming that the delay of fluorescence is linear with shelving time the error is only of order 30 μs. We note that there were no soft edges in the runs used for our final data set.

We found that a horizontal field gave a much smaller heating effect, and indeed some of our final data points were taken in the presence of a horizontal field of order 200 V/m. However, for our final experimental run, a further beam was introduced along $(0, -2, -1)$ to allow horizontal field compensation; this beam was blocked once the compensation was optimised. Although not important for the present lifetime measurements, accurate compensation is necessary for our future work in which the ion is to be cooled below the Doppler limit.

4.2.2 Tests of the reliability of the data analysis

We consider three possible sources of systematic error in the data analysis in turn. First, it is straightforward to show analytically that approximating the continuous ex-

ponential distribution of dark times as a histogram causes no systematic errors in the fitted value of τ. Second, numerically simulated data was used to show that varying the threshold level used in the data analysis, did not systematically change the fitted value of τ by more than 0.1 ms. Our real data has a further property: intensity fluctuations. The τ value deduced from a real data set was found to vary as a function of threshold by amounts of order ± 0.5 ms. We estimate this may introduce a systematic error of order 0.5 ms. Third, repeated fits to numerically simulated data sets were used to show that any systematic error arising purely from the exponential fitting procedure was less than 0.25 ms. They also permitted us to verify the uncertainty (one standard deviation) in the fitted value of τ, derived from the cost function surface.

These effects give a total uncertainty of ± 0.6 ms.

5 Demonstration of photon antibunching

The quantum jump method provides a convenient means to demonstrate photon antibunching [22], that is, generation of a light field whose second order coherence $g^{(2)}(t)$ falls below 1 as $t \to 0$. The second-order coherence is the normalised autocorrelation function of the intensity. A classical definition of intensity leads to $g^{(2)}(t) < g^{(2)}(0)$ and $g^{(2)}(0) > 1$, whereas a definition in terms of quantum electric field operators allows all values [22]. Therefore observation of a $g^{(2)}(0)$ value below 1 is a direct signature of the quantum nature of the radiation field. Quantum jump observations yield $g^{(2)}$ easily, since whenever a de-shelving jump is observed, we may deduce, with close to 100% reliability, that one photon at 729 nm has been emitted by the ion [23]. Therefore we deduce the presence of a 729 nm radiation field which has $g^{(2)}(t) = \langle n(t)n(0)\rangle / \bar{n}^2$, where $n(t)$ and $n(0)$ are the numbers of jumps observed in two equal time intervals separated by a time t. This quantity is plotted in figure 8 for a typical data set in our experiment. For this study, we did not use the method described in section 2, in which the 850 nm light was blocked when the ion was shelved. Instead, this light was left permanently on, and the fluorescence monitored continuously. We therefore obtained the well-known 'random telegraph' signal, figure 3b. Since we detect very close to all the 729 nm photons, we can be confident the second order coherence does not vary at time-scales too short for us to detect. Therefore the antibunching signature $g^{(2)}(0) < 1$ is clearly demonstrated.

We can understand the complete form of $g^{(2)}(t)$ by solving the rate equations for the populations of the ion's levels. All the relevant processes are fast except for two, namely spontaneous decay from $D_{5/2}$ to Λ and excitation from Λ to $D_{5/2}$, so the problem reduces to a two-level system. If we take $t = 0$ to be the centre of a short time interval (one bin) during which a jump occurred, so that $n(0) = 1$, then the probability for the atom to emit a 729 nm photon at time t is proportional to the population of $D_{5/2}$ at t, given that it was zero at $t = 0$. We thus obtain

$$g^{(2)}(t) = 1 - e^{-(R+\gamma)t} \tag{5}$$

where R is the excitation rate, γ the decay rate. This curve is plotted on figure 8 with no free parameters (R is taken as the inverse of the mean duration of bright periods in the same data set). The agreement between data and theory is evidence that we have a good understanding of our experimental situation.

6 Result and discussion

Our final data set consisted of four 8-hour runs, and two 2-hour runs, all using the experimental method of section 2 (850 nm laser blocked during dark periods). The de-shelving rates observed in these runs, as obtained by the analysis described above, are shown in figure 7b. The size of each error bar is equal to the statistical uncertainty emerging from the analysis. The straight line through the data is a single-parameter weighted least-squares fit. The line is given the theoretically expected slope, and the best fit intercept is found to be $\gamma_0 = 0.856 \pm 0.004\ \mathrm{s}^{-1}$.

The de-shelving rate γ obtained in the experiment may be written

$$\gamma = \frac{1}{\tau} + \sum_i \gamma_i \tag{6}$$

where τ is the natural lifetime we wish to measure, and the γ_i are due to other processes which contribute to the measured rate, chiefly laser excitation of transitions in the ion and collisional processes. The effect of off-resonant excitation by 866nm radiation is already accounted for in our fitted intercept γ_0. However, uncertainty ($\pm 30\%$) in the light intensity at the ion makes this accounting imprecise, leading to a further systematic error in γ_0 at the level of $0.001\,\mathrm{s}^{-1}$. This and other contributions to the systematic error, from collisional processes and remaining background light from the 866nm laser, are shown in Table 1. The statistical error from the data fitting dominates. The systematic effects are independent of one another, so we add their errors in quadrature. Adding this total systematic error linearly to the statistical error, the value we obtain for the natural lifetime of the $D_{5/2}$ level is

$$\tau = 1.168 \pm 0.007\ \mathrm{s} \tag{7}$$

We have already noted the significant difference between this result and earlier measurements. Here we compare it with theory. Our result differs from all the reported *ab initio* calculations by amounts large compared with our 0.6 % experimental uncertainty. The relative difference $(\tau_{\mathrm{theor.}} - \tau_{\mathrm{meas.}})/\tau_{\mathrm{meas.}}$ is -10% for a recent calculation based on the Brueckner approximation [7], $+5.6\%$ for relativistic many-body perturbation theory [4], and -2.6% for multi-configurational Hartree Fock (MCHF) calculations [5, 6]. Of these calculations, those which produced

effect	1σ errors ($10^{-3}\,\mathrm{s}^{-1}$)	
	statistical	systematic
data fitting	± 4	± 0.4
866nm intensity uncertainty (30%)		± 1
A_{21} uncertainty (4%)		± 0.1
collisional processes		± 0.6
background from 866nm laser		$\sim +0.01$
total	± 4	± 1.2

Table 1: Statistical and systematic contributions to the error in the measured de-shelving rate γ. The systematic errors are added in quadrature, then their total is added linearly to the statistical error, to give a total uncertainty of $5.2 \times 10^{-3}\,\mathrm{s}^{-1}$. See also section 4.

the smallest discrepancy with our measured D state lifetime produced the largest discrepancy with the measured P state lifetimes obtained by Jin and Church [11]. A semi-empirical calculation based on MCHF and core polarization [5], and a calculation using related methods [6], give a value close to our measured result (relative difference -0.7%). The most natural interpretation of these observations is that the *ab initio* calculations of τ carried out so far have a precision of at best a few percent, and success at calculating electric dipole matrix elements does not guarantee the same degree of success with other parameters such as electric quadrupole matrix elements.

The ratio between the lifetimes of $D_{3/2}$ and $D_{5/2}$ is much less sensitive to imperfections in the calculations, and is given primarily by the frequency factor ω^5, which leads to a ratio 1.022. The factor emerging in recent calculations of the two lifetimes is 1.0335 [7], 1.0283 [4], 1.0175 [5, 6]. We take the standard deviation of these results to indicate the theoretical uncertainty on their mean, giving $\tau_{3/2}/\tau_{5/2} = 1.026 \pm 0.007$. Combining this with our measurement of $\tau_{5/2}$ gives $\tau_{3/2} = 1.20 \pm 0.01$ s for the lifetime of the $3d\,^2D_{3/2}$ level in $^{40}\mathrm{Ca}^+$.

7 Conclusion

We have described a new linear ion trap apparatus and its use to measure the lifetime of the $D_{5/2}$ level in $^{40}\mathrm{Ca}^+$ by quantum jump measurements on a single trapped ion. Our result is more precise than previous measurements, and significantly larger. We believe this discrepancy is mostly explained by previously unrecognised systematic errors, which tend to make the lifetime appear shorter than it in fact is. Our measurement provides a new precise test of *ab initio* atomic structure calculations; it is in only moderate agreement with currently reported calculations.

We have discussed the spectral distribution of light emitted by a semiconductor diode laser operated in an extended cavity, emphasizing that in experiments where unwanted excitation of allowed atomic transitions is to be avoided, it is necessary to take into account the weak broad component in the spectrum, which extends many nanometres away from the main lasing wavelength. This is significant in many experiments in atomic physics, especially coherent atom optics, 'dark' optical lattices, frequency standards and quantum information processing.

Finally, we have discussed various diagnostics on the performance of the ion trap, made possible by careful analysis of long periods of operation of the trap. These include an upper limit for the pressure in the system, and the heating rate in the trap. We demonstrated photon anti-bunching, finding it in agreement with theoretical expectations.

Our uncertainty is dominated by statistics, so it would be possible to obtain significantly higher precision by accumulating more data, though for single-ion work this would require integration for several weeks. To go further, one would need better knowledge of the laser intensities and collisional processes.

8 Acknowledgements

We would like to acknowledge helpful correspondence with G. Werth, and a preprint of [12]. L. Favre, E. Hodby, M. McDonnell and J. P. Stacey contributed to development of the apparatus, D. T. Smith designed the high voltage r.f. supply, and we are grateful for general technical assistance from G. Quelch. We thank R. Blatt and the Innsbruck group (especially F. Schmidt-Kaler, C. Roos, M. Schulz) for many helpful discussions and guidance, and similarly R. C. Thompson and D. N. Segal. This work was supported by EPSRC (GR/L95373), the Royal Society, Riverland Starlab and Oxford University (B(RE) 9772).

References

[1] F. Plumelle, M. Desaintfuscien, and M. Houssin, IEEE Transactions on Instrumentation and Measurement **42**, 462 (1993).

[2] M. A. Ali and Y. Kim, Phys. Rev. A **38**, 3992 (1988).

[3] C. J. Zeippen, Astron. Astrophys. **229**, 248 (1990).

[4] C. Guet and W. R. Johnson, Phys. Rev. A **44**, 1531 (1991).

[5] N. Vaeck, M. Godefroid, and C. Froese-Fischer, Phys. Rev. A **46**, 3704 (1992).

[6] T. Brage, C. Froese-Fischer, N. Vaeck, M. Godefroid, and A. Hibbert, Physica Scripta **48**, 533 (1993).

[7] S. S. Liaw, Phys. Rev. A **51**, R1723 (1995).

[8] E. Biemont and C. J. Zeippen, Comments on At. Mol. Phys. **33**, 29 (1996).

[9] D. E. Osterbrock, *Astrophysics of Gaseous Nebulae* (Freeman, San Francisco, 1974).

[10] S. C. Bennett and C. E. Wieman, Phys. Rev. Lett. **82**, 2484 (1999).

[11] J. Jin and D. A. Church, Phys. Rev. Lett. **70**, 3213 (1993).

[12] M. Block, O. Rehm, P. Seibert, and G. Werth, The European Physical Journal D **7**, 461 (1999).

[13] S. Bourzeix, M. D. Plimmer, F. Nez, L. Julien, and F. Biraben, Optics Communications **99**, 89 (1993).

[14] C. S. Adams and A. I. Ferguson, Opt. Comm. **90**, 89 (1992).

[15] G. D. Boyd and D. A. Kleinman, Journal of Applied Physics **39**, 3597 (1968).

[16] Technical report, Casix Inc. (private communication).

[17] C. E. Theodosiou, Phys. Rev. A **39**, 4880 (1989).

[18] J. C. Camparo, Contemporary Physics **26**, 443 (1985).

[19] M. de Labachelerie and P. Cerez, Optics Communications **55**, 174 (1985).

[20] F. Arbes, T. Gudjons, F. Kurth, G. Werth, F. Marin, and M. Inguscio, Zeitschrift fur Physik D **25**, 295 (1993).

[21] F. Arbes, M. Benzing, T. Gudjons, F. Kurth, and G. Werth, Zeitschrift fur Physik D **31**, 27 (1994).

[22] R. Loudon, *The Quantum Theory of Light* (Oxford University Press, 1995).

[23] J. C. Bergquist, R. G. Hulet, W. M. Itano, and D. J. Wineland, Phys. Rev. Lett. **57**, 1699 (1986).

[24] M. Knoop, M. Vedel, and F. Vedel, Phys. Rev. A **52**, 3763 (1995).

[25] T. Gudjons, B. Hilbert, P. Seibert, and G. Werth, Europhysics Letters **33**, 595 (1996).

[26] G. Ritter and U. Eichmann, Journal of Physics B - Atomic Molecular and Optical Physics **30**, L141 (1997).

[27] J. Lidberg, A. Al-Khalili, L.-O. Norlin, P. Royen, X. Tordoir, and S. Mannervik, Journal of Physics B **32**, 757 (1999).

Arbes *et al.* 1994	[21]	1054(61)
Knoop *et al.* 1995	[24]	994(38)
Gudjons *et al.* 1996	[25]	1064(17)
Ritter *et al.* 1997	[26]	969(21)
Lidberg *et al.* 1999	[27]	1090(50)
Block *et al.* 1999	[12]	1100(18)
This work		1168(7)
Ali & Kim 1988	[2]	950
Zeippen 1990	[3]	1053
Guet & Johnson 1991	[4]	1236
Vaeck *et al.* 1992	[5]	1140
Brage *et al.* 1993	[6]	1163
Liaw 1995	[7]	1045
Biemont & Zeippen 1996	[8]	1070

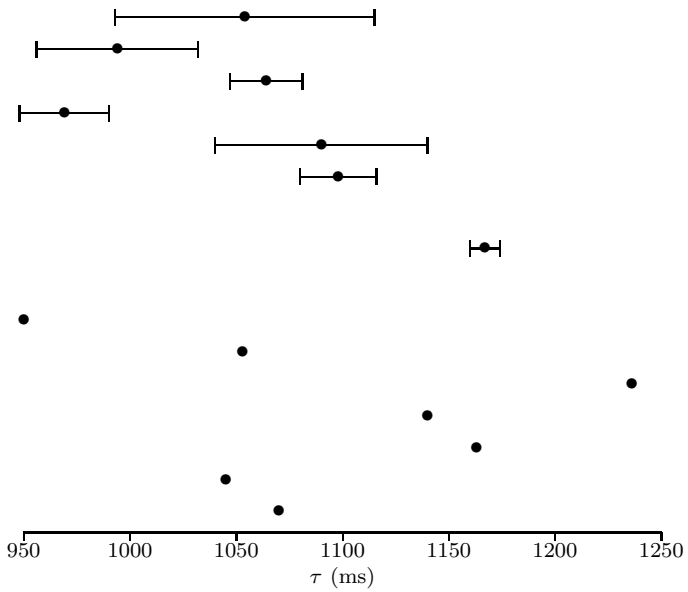

Figure 1: Values of τ experimentally measured (points with error bars) and theoretically calculated *ab initio* (circles). The first two columns give the reference, the third gives τ in milliseconds. Earlier measured values are not shown since they have considerably larger experimental uncertainty.

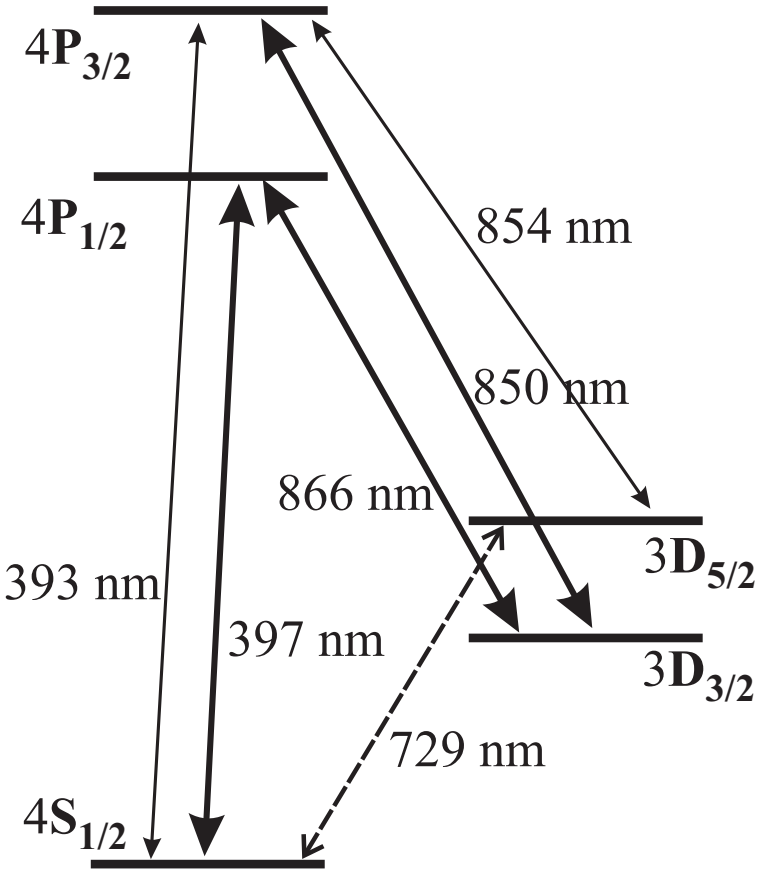

Figure 2: Low-lying energy levels of $^{40}Ca^{+}$ and associated transitions. Lasers at 397 nm, 866 nm and 850 nm drive the corresponding transitions in the experiments. The other transitions are significant to the interpretation of the measured signals and to systematic effects.

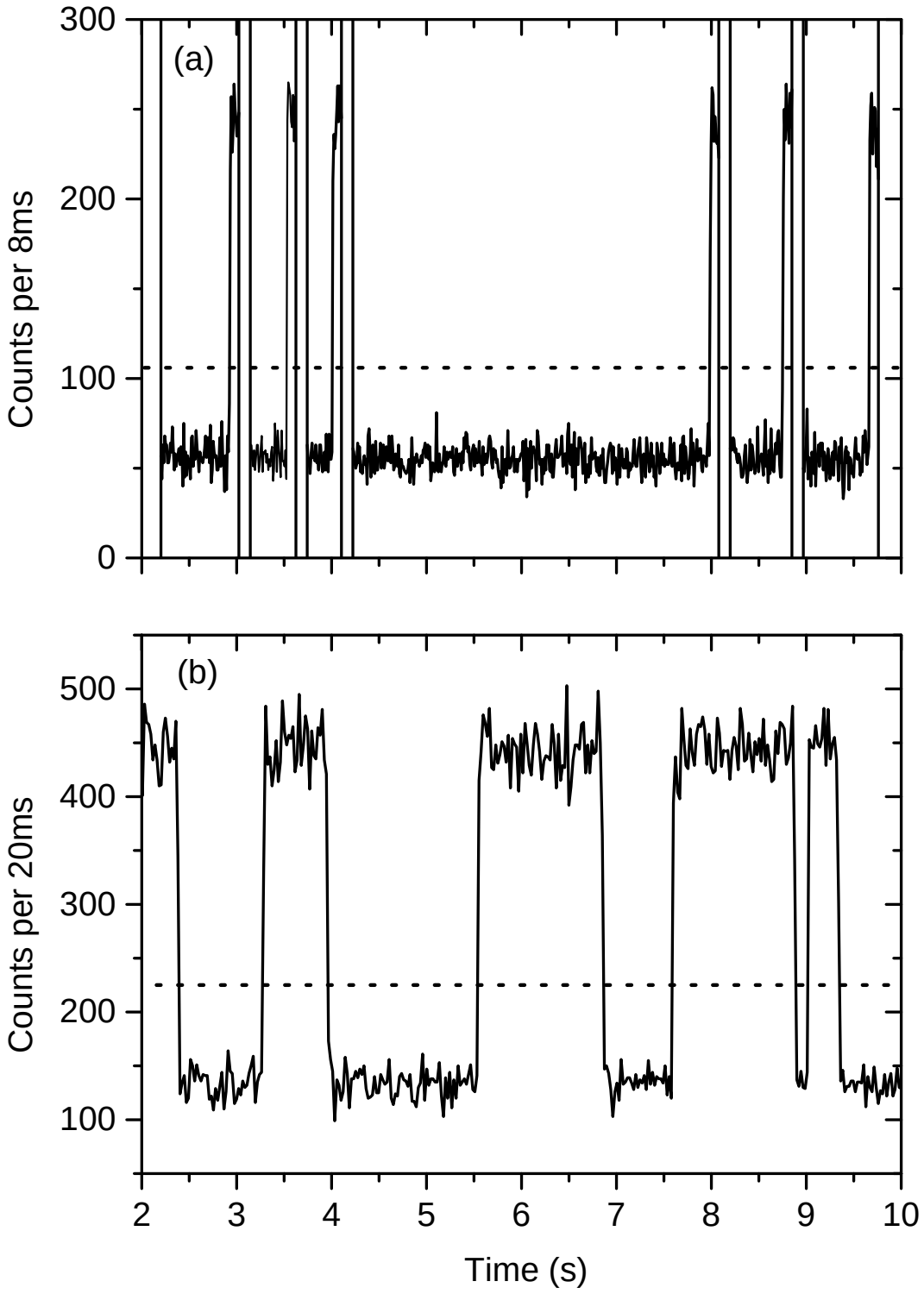

Figure 3: Observed fluorescence signals. The vertical axis is the number of counts given by the photomultiplier during one counting bin, the horizontal axis is time. The horizontal dashed lines show the threshold settings for the data analysis. (a) Shutter method, in which 850 nm laser is blocked during dark periods. The vertical lines indicate shutter opening and closing events. (b) Random telegraph method, in which 850 nm laser is permanently on. (a) was used for accurate τ measurements, (b) for $g^{(2)}$ measurements and various systematic studies.

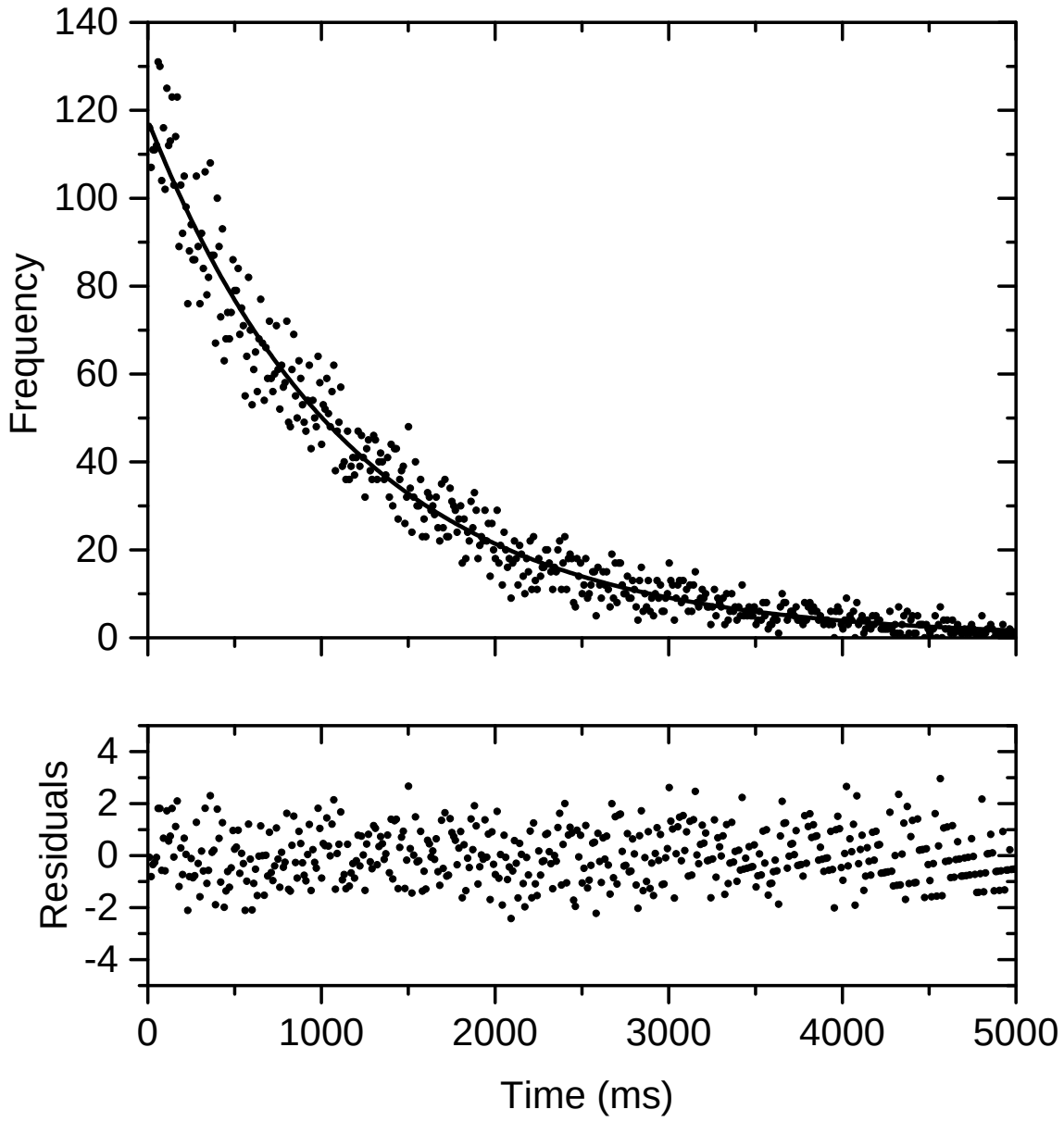

Figure 4: Typical data set from a single 8-hour run. The figure shows a histogram of the measured dark period durations x_i, and the fitted exponential curve produced by our analysis procedure (see text). The residuals are shown on an expanded scale, in the form (data−fit)/$\sqrt{}$(fit). In this example the analysis gave $A = 117.7 \pm 1.5$, $\gamma = 0.853 \pm 0.009$.

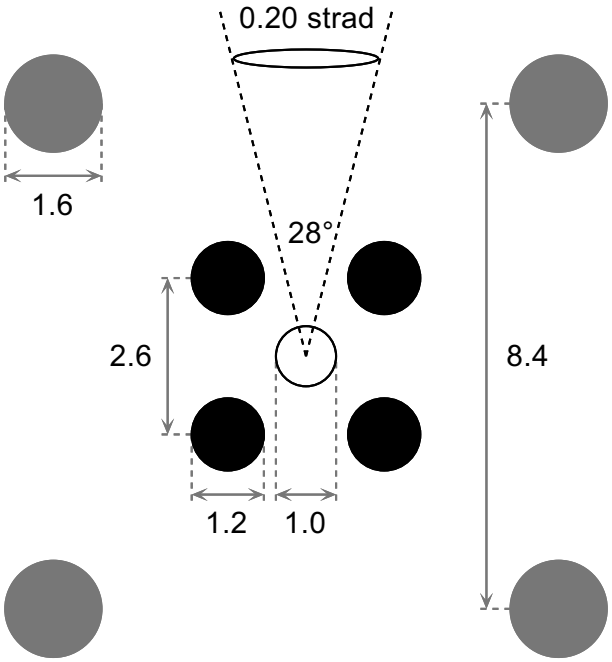

Figure 5: End view of the linear ion trap electrode arrangement, to scale, showing the a.c. trap electrodes (solid black circles) and d.c. compenstation electrodes (grey circles). Dimensions are in mm. The position of the d.c. endcaps is also indicated (open circle); the separation between the two opposing endcaps is 7.2 mm. The solid angle in which fluorescence is collected by the imaging system is 0.2 steradians.

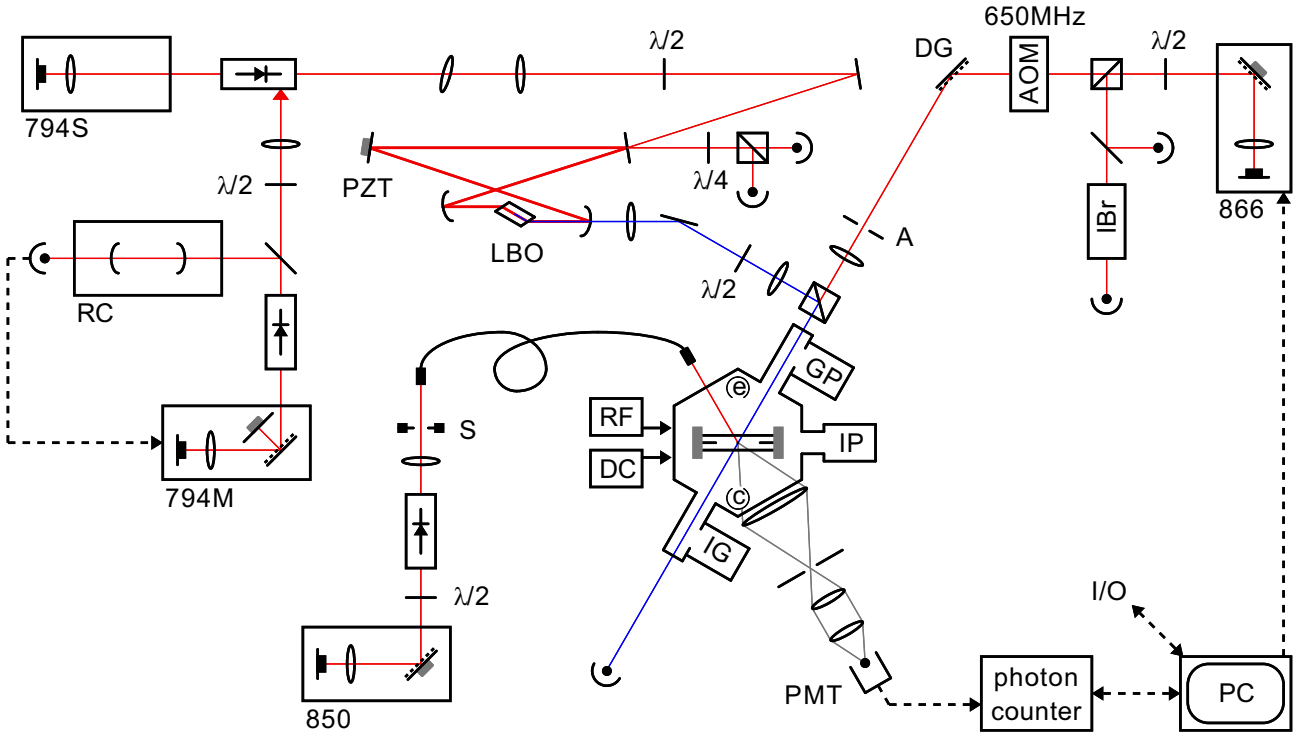

Figure 6: Main features of the optical set-up; see section 3 for key.

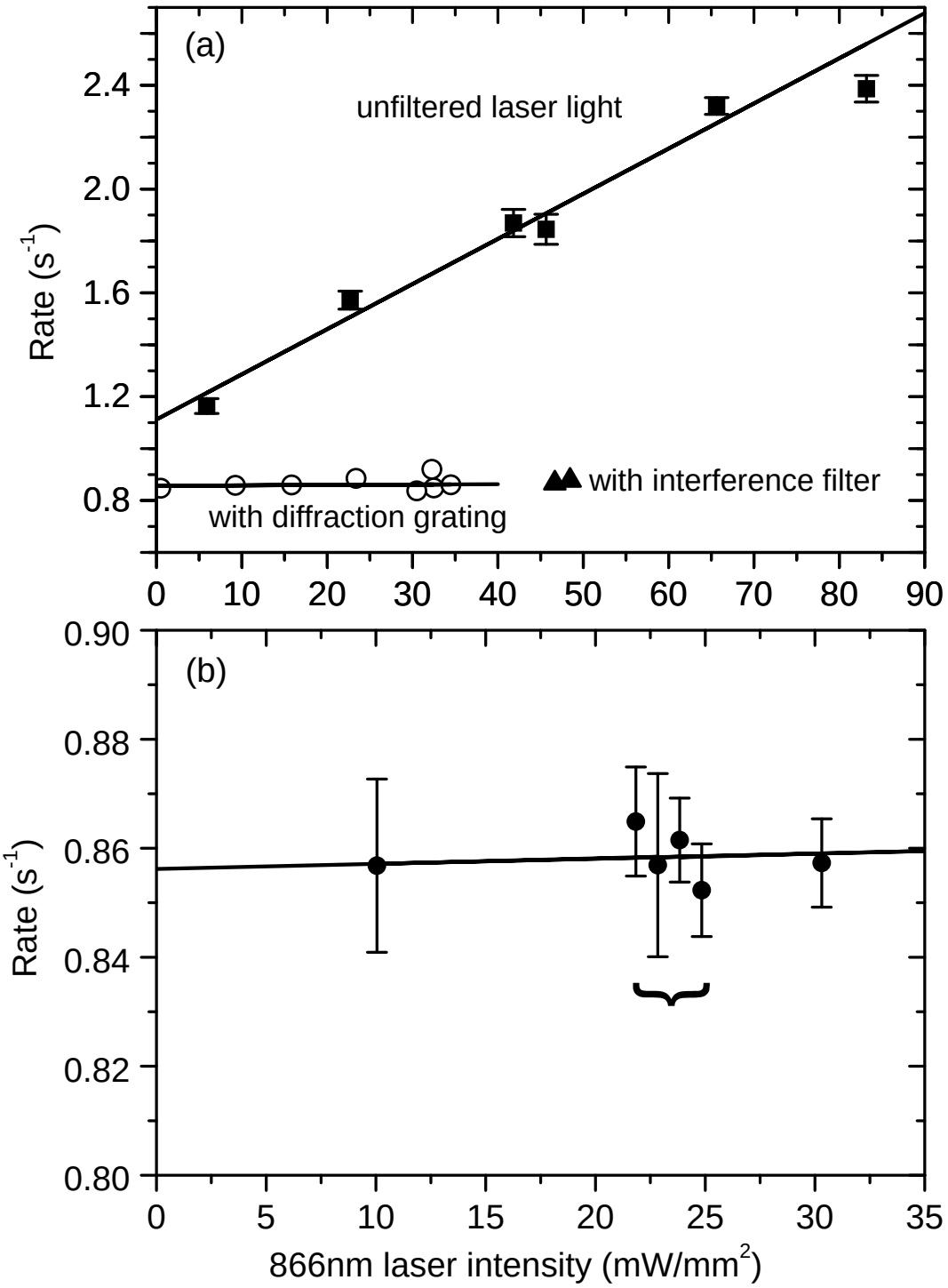

Figure 7: Measured de-shelving rates. (a) Measurements using 1 to 2 hour runs of the random telegraph method, at various 866 nm beam intensities, to test for intensity dependence of the rate. The lines are 2-parameter straight line fits to the data, with fitted intercept and slope. With the diffraction grating and aperture in place, the slope is consistent with zero and with the small theoretically expected value (see text). (b) Final data set using the shutter method. Points taken at the same intensity are shown horizontally offset for clarity. The error bars are the statistical uncertainties emerging from the analysis of each run. The line is a single-parameter least-squares fit; it is given the theoretically expected slope, and the best fit intercept is obtained.

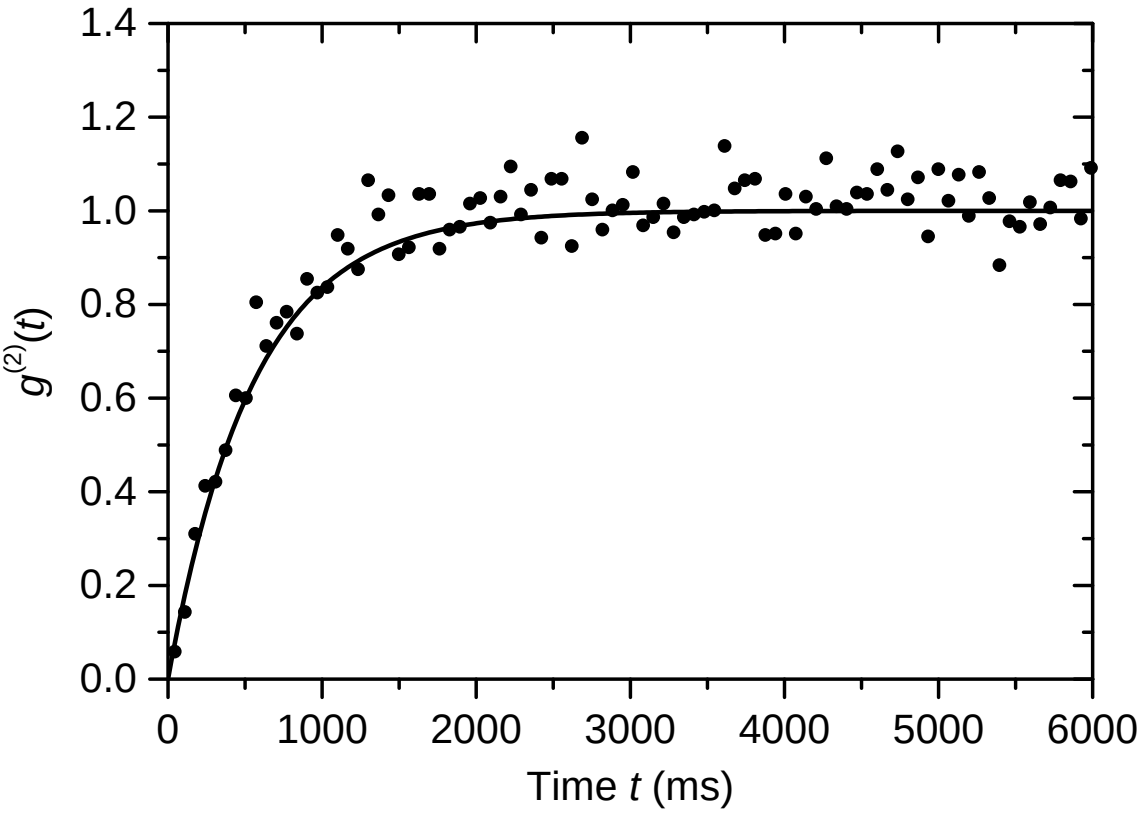

Figure 8: Second-order coherence of the 729 nm radiation emitted by the ion, as deduced from quantum jump observations. The data points give the number of times a jump was observed (therefore a 729 nm photon emitted) at time t after a chosen jump, normalised to the mean jump rate, accumulated in several data sets. The line is the theoretical expectation, described in the text.